

Ergodicity Breaking in Thermal Biological Electron Transfer? Cytochrome C Revisited II

Zdenek Futera,[†] Xiuyun Jiang,[‡] and Jochen Blumberger^{*,‡}

*[†]Faculty of Science, University of South Bohemia, Branisovska 1760, 370 05 Ceske
Budejovice, Czech Republic.*

*[‡]Department of Physics and Astronomy and Thomas Young Centre, University College
London, London WC1E 6BT, UK.*

E-mail: j.blumberger@ucl.ac.uk(J.B.)

Phone: ++44-(0)20-7679-4373. Fax: ++44-(0)20-7679-7145

Abstract

It was recently suggested that cytochrome c operates in an ergodicity-breaking regime characterized by unusually large energy gap thermal fluctuations and associated reorganization free energies for heme oxidation of up to 3.0 eV. The large fluctuations were reported to lower activation free energy for oxidation of the heme cofactor by almost a factor of 2 compared to the case where ergodicity is maintained. Our group has recently investigated this claim computationally at several levels of theory and found no evidence for such large energy gap fluctuations. Here we address the points of our earlier work that have raised criticism and we also extend our previous investigation by considering a simple linear polarizability model for cytochrome c oxidation. We find very consistent results among all our computational approaches, ranging from classical molecular dynamics, to the linear polarizability model to QM(PMM)/MM to full QM(DFT)/MM electrostatic embedding. None of them support the notion of unusually large energy gap fluctuations or ergodicity breaking. The deviation between our simulations and the ones reported in [*J. Phys. Chem. B* **2017**, 121, 4958] is traced back to an unusually large electric field at the Fe site of the heme c cofactor in that study, not seen in our simulations, neither with the AMBER nor with the CHARMM force field. While ergodicity breaking effects may well occur in other biological ET, our numerical evidence suggests that this is not the case for cytochrome c.

Introduction

Biological electron transfer (ET) processes are typically mediated by redox proteins incorporating metal cations in their cofactors. Such processes are often well described by Marcus theory of electron transfer where free energy curves of the initial and final states have parabolic shapes and the free energy barrier for electron transfer is described by only two parameters, driving force ΔA and the reorganization free energy λ . In more general theories, one distinguishes between two reorganization free energies, the variational reorganization free energy λ_M^{var} ($M = \text{R}, \text{O}$ denoting reduced or oxidized state) determining the curvature of the free energy curves and the Stokes reorganization free energy, λ^{st} , determining the horizontal shift of their minima.¹ However, assuming linear response, on which the Marcus theory is based, these two parameters are the same and this turned out to be a good approximation for ET in various biomolecules.¹⁻¹⁸

Nevertheless, there are well-known exceptions for which the Marcus picture does not hold, for instance when the vertical energy gap ΔE , used as the reaction coordinate for the free energy curves, does not follow a Gaussian distribution or when the phase space is not sampled according to the Boltzmann distribution, i.e. not ergodically.¹ The non-Gaussian gap distributions are typical for ET from/to apolar particles,¹⁹ redox couples with different solvation-shell coordination numbers²⁰⁻²² or for solutes with a strong polarizability difference in oxidized and reduced state.²³⁻²⁶ On the other hand, non-ergodicity is related to ultrafast ET (picoseconds or sub-picoseconds time scales) or to systems with very slow motions (microsecond and longer time scales) coupling to ET.^{10,24-26} While in the former case the separation between electron and nuclear dynamics can no longer be made and should ideally be treated with quantum dynamical methods, the latter case needs very long molecular dynamics (MD) simulations or separate long-time scale simulations of relevant structural conformations.

Matyushov and co-workers argued in series of papers that the latter type of ergodicity-breaking has a profound impact on the kinetics of ET by lowering the activation free energy

barrier for ET.^{10,23,24,27–31} Due to the incomplete relaxation of the protein on the timescale of the ET event, the Stokes reorganization free energy λ^{st} is no longer the same as the variational λ^{var} related to thermal fluctuations of the vertical energy gap but significantly smaller, $\lambda^{\text{st}} \ll \lambda^{\text{var}}$, resulting in a lowering of the ET activation free energy by a factor $\lambda^{\text{var}}/\lambda^{\text{st}}$ for parabolic free energy profiles.¹⁰

The non-ergodic effect described above was demonstrated for oxidation of the Fe-heme cofactor in cytochrome c, where unusually high values for λ^{var} , as large as 3.0 eV, were reported, while estimates for λ^{st} were significantly smaller, 1.3 eV^{28–30} Motivated by these curious results, we investigated the same system at various levels of theory including (i) classical MD simulations with additive and electronically polarizable force fields, (ii) hybrid QM(PMM)/MM calculations based on the perturbed matrix method (PMM) and ZINDO/S electronic-structure calculations, and (iii) QM(DFT)/MM calculations with the QM region treated by full electrostatic DFT embedding.³² All approaches provided consistent results and similar values for the two reorganization free energies, $\lambda^{\text{st}} = 0.9 - 1.0$ eV, $\lambda^{\text{var}} = 0.9 - 1.3$ eV with electronically non-polarizable force fields. None of these methods gave evidence for ergodicity-breaking effects for oxidation of cytochrome c. Instead, the oxidation/reduction kinetics was found to be in line with standard Marcus theory and in good agreement with electrochemically determined reorganization free energy when an electronically polarizable protein and water force field was used.

In a recent publication, Martin, Dinpajoooh and Matyushov (MDM)³¹ criticized our QM(PMM)/MM calculations³² for neglecting the diagonal dipole moments in the PMM Hamiltonian and for apparent misalignment of the QM and MM molecular coordinate frames when calculating the interaction with the protein electric field. In the present work we show that diagonal dipole-moment elements of the PMM Hamiltonian have very little effect on the vertical energy gap distributions and we add an explanation how the protein electric field was rotated into the coordinate frame of the cofactor. Moreover, we show that the simple linear polarizability model investigated by MDM in Ref. 31 gives results that are very similar

to QM(PMM)/MM. Hence, QM(PMM)/MM, its simpler linear polarizability approximation and our highest level QM(DFT)/MM calculations give consistent results none of them showing evidence for non-ergodic effects in cytochrome c. The unusually large variance reorganization free energy reported by MDM are traced back to large electric fields at the Fe site not seen in our molecular dynamics simulations.

Computational Details

All calculations carried out in this article use the classical molecular dynamics (MD) data reported in Ref. 32 for horse heart cytochrome (pdb id 1GIW).³³ In our previous work the simulation was set up as described in Ref. 29,30 to ensure comparability of the data generated by MDM and us. Briefly, the protein was described with the CHARMM27 force field,³⁴ surrounded by a cubic box ($a = 101.08 \text{ \AA}$) of TIP3P water³⁵ and treated in periodic boundary conditions. Production runs in the NVT ensemble of length 250 ns MD simulation were performed using a 2 fs time step and the SHAKE algorithm to constrain bonds including hydrogens. The Particle Mesh Ewald (PME) technique with real-space cutoff 12 \AA was used to evaluate the electrostatic energy and a target temperature of 290 K was imposed by Langevin thermostat. The NAMD software³⁶ was employed to run the classical MD simulations. Perturbed matrix method (PMM)³⁷⁻⁴¹ calculations were done on $\sim 28\,000$ MD configurations extracted from the production run described above. Unperturbed excitation energies $\epsilon_i^{(M)}$ and transition dipoles $\mu_{ij}^{(M)}$ were obtained using ZINDO/S calculations on reduced ($M = R$) and oxidized ($M = O$) protein active-site structure. In this work we also report diagonal dipole moments $\mu_{ii}^{(M)}$ at ZINDO/S level, see SI for numerical values and active site coordinates. All ZINDO/S calculations were carried out with the Gaussian 16 package.⁴²

Results and Discussion

QM(PMM)/MM calculations

In a recent paper, MDM claimed that one of our lower-level calculations, QM(PMM)/MM, was erroneous.³¹ Specifically, they claimed that (1) we “failed to rotate the vector of the electric field of the protein-water medium to the molecular frame of the active site” and (2) we “neglected the diagonal dipole moments in the PMM Hamiltonian matrix.”

Claim (1) is untrue and the result of an unfortunate misinterpretation of our raw data for electric field fluctuations that we provided upon their request. In the following we define the PMM Hamiltonian and describe how the electric field vector was rotated into the molecular frame. In PMM^{37–41} the potential energy of the redox state M ($M = \text{R}$ or O) are obtained from electronic structure calculations on the QM center in vacuum, here the Fe-heme cofactor including axial ligands. The interaction with the electrostatic field generated by the protein atoms and water is calculated perturbatively via a multipole expansion of the QM center, usually truncated at second order,

$$H_{ij}^{(M)} = (\epsilon_i^{(M)} + Q_{\text{Fe}}^{(M)} V_{\text{Fe}}) \delta_{ij} - \boldsymbol{\mu}_{ij}^{(M)} \cdot \mathbf{E}_{\text{Fe}} \quad (1)$$

$$E_M = \text{Min}[\{EV_i(\mathbf{H}^{(M)})\}], \quad M = \text{R}, \text{O}, \quad (2)$$

where $\mathbf{H}^{(M)}$ is the perturbed Hamiltonian matrix for oxidation state M with matrix elements $H_{ij}^{(M)}$, $\epsilon_i^{(M)}$ are the unperturbed ground and excited electronic state energies of the heme cofactor in vacuum, $Q_{\text{Fe}}^{(M)}$ is the total charge of the QM region in redox state M assumed to be located on the Fe atom (i.e., $Q_{\text{Fe}}^{(\text{O})} = -1e$, $Q_{\text{Fe}}^{(\text{R})} = -2e$), V_{Fe} is the Coulomb potential and $\mathbf{E}_{\text{Fe}} = -\nabla V|_{\text{Fe}}$ the corresponding electric field on the Fe atom due to the MM atoms, and $\boldsymbol{\mu}_{ij}^{(M)} = -e\langle\phi_i|\mathbf{r}|\phi_j\rangle$ are the dipole moment ($i=j$) and transition dipole moment ($i \neq j$) matrix elements obtained from QM calculations in gas phase. The potential energy of redox state M , E_M , is the lowest eigenvalue (EV) of $\mathbf{H}^{(M)}$ and used for the calculation of the

vertical energy gap between oxidized and reduced state, ΔE ,

$$\Delta E(\mathbf{R}^N) = E_O(\mathbf{R}^N) - E_R(\mathbf{R}^N). \quad (3)$$

where we have explicitly indicated the dependence of these energies on the coordinates of all atoms, \mathbf{R}^N .

In Ref. 32 the transition dipoles $\boldsymbol{\mu}_{ij}^{(M)}$ were calculated in the so-called standard orientation of the electronic-structure programme Gaussian, where the center of nuclear charge is translated to the origin of the the Gaussian Cartesian coordinate system (\mathbf{X} , \mathbf{Y} , and \mathbf{Z}) and the main symmetry axis is rotated to align with the \mathbf{Z} direction (axes in red in Fig. 1). The coordinates of the reduced and oxidized heme model in this frame are given in Tables S1-S2. For each MD snapshot, the electric field vector at the Fe site was first calculated in the space fixed coordinate system used in the MD simulation of the full aqueous protein (\mathbf{X}' , \mathbf{Y}' , \mathbf{Z}' , not shown), denoted \mathbf{E}'_{Fe} , and then rotated to the Gaussian (\mathbf{X} , \mathbf{Y} , \mathbf{Z}) frame, giving \mathbf{E}_{Fe} . For the rotation from the MD to the Gaussian frame, we defined a local heme coordinate frame (\mathbf{x} , \mathbf{y} , \mathbf{z} , axes in blue in Fig. 1). The latter is defined by two vectors $\mathbf{x}' = \mathbf{R}_{\text{NC}} - \mathbf{R}_{\text{NA}}$ and $\mathbf{y}' = \mathbf{R}_{\text{ND}} - \mathbf{R}_{\text{NB}}$ where NA, NB, NC and ND are the four nitrogen atoms of the heme ring. The axes \mathbf{x} and \mathbf{y} were obtained by symmetric orthonormalization of \mathbf{x}' and \mathbf{y}' and the third axis \mathbf{z} was chosen orthonormal to \mathbf{x} and \mathbf{y} . The rotation matrix transforming from the MD to the Gaussian frame is then

$$\mathbf{R} = \mathbf{G}\mathbf{M}^{-1} \quad (4)$$

where the columns of \mathbf{G} and \mathbf{M} are the unit vectors along \mathbf{x} , \mathbf{y} , \mathbf{z} in the (\mathbf{X} , \mathbf{Y} , \mathbf{Z}) and (\mathbf{X}' , \mathbf{Y}' , \mathbf{Z}') coordinate frames. The electric field vector in the Gaussian frame is then given by

$$\mathbf{E}_{\text{Fe}} = \mathbf{R}\mathbf{E}'_{\text{Fe}}. \quad (5)$$

Claim (2) is true but we find here that inclusion of the diagonal elements of the transition moment matrix (i.e. dipole moments), $\boldsymbol{\mu}_{ii}$, has only a negligible effect. We calculated the dipole moments in the (\mathbf{X} , \mathbf{Y} , \mathbf{Z}) frame using Gaussian (Tables S3-S6 for the reduced and oxidized heme states). The reorganization energies obtained with and without $\boldsymbol{\mu}_{ii}$ are summarized in Tab. 1. From (1) we obtain $\lambda_{\text{R}}^{\text{var}} = 1.27$ eV and $\lambda_{\text{O}}^{\text{var}} = 1.29$ eV using the MD configurations labeled “QM2/SF1” in Ref. 32, which is very close to our previous results where the diagonal terms $\boldsymbol{\mu}_{ii}$ were omitted, $\lambda_{\text{R}}^{\text{var}} = 1.23$ eV and $\lambda_{\text{O}}^{\text{var}} = 1.24$ eV, respectively. λ^{st} is hardly affected either increasing from 1.00 to 1.03 eV when the diagonal elements are included. All these changes are well within the statistical error bar of our calculations. On the contrary, MDM reported a large increase in $\lambda_{\text{R}}^{\text{var}}$ upon inclusion of $\boldsymbol{\mu}_{ii}$ when they used our raw data for the electric field (“EVB MF (no rot, zero dipoles)” vs “EVB MF (no rot)” in Table 2 of Ref. 31). This is most likely related to the unfortunate misinterpretation of our electric field raw data, since our $\boldsymbol{\mu}_{ii}$ values are consistent with MDM data.³¹

Linear polarizability model

Our results obtained from QM(PMM)/MM calculations are further confirmed by the simpler linear polarizability model that was investigated by MDM in Ref. 31. In this model, the solvent-induced shift of the energy gap is expressed as a perturbation truncated at second order,

$$\Delta E(\mathbf{R}^N) = -\Delta Q V_{\text{Fe}}(\mathbf{R}^N) + \frac{1}{2} \mathbf{E}_{\text{Fe}}(\mathbf{R}^N) \cdot \boldsymbol{\Delta\alpha} \cdot \mathbf{E}_{\text{Fe}}(\mathbf{R}^N) \quad (6)$$

where $\Delta Q = Q_{\text{R}} - Q_{\text{O}}$ and $\boldsymbol{\Delta\alpha}$ is the polarizability difference tensor,

$$\boldsymbol{\Delta\alpha} = \boldsymbol{\alpha}_{\text{R}} - \boldsymbol{\alpha}_{\text{O}} \quad (7)$$

and α_M the polarizability tensor for reduced ($M = \text{R}$) and oxidized state ($M = \text{O}$), with elements

$$[\alpha_M]_{k,l} = \alpha_M^{k,l} = 2 \sum_{i=1}^N \frac{\mu_{0i,k}^{(M)} \cdot \mu_{i0,l}^{(M)}}{\epsilon_i^{(M)} - \epsilon_0^{(M)}}, \quad k, l = 1, 2, 3. \quad (8)$$

Here and in the following we use the same notation as MDM, except that we define the energy gap ΔE in Eq. 6 with opposite sign to remain consistent with (3) and our previous works.³² It follows from (6) that the energy gap fluctuations in state M , $\delta E = \Delta E - \langle \Delta E \rangle_M$, can be decomposed in potential (V) and field (F) contributions,

$$\delta E = \delta E^V + \delta E^F \quad (9a)$$

$$\delta E^V = e(V_{\text{Fe}} - \langle V_{\text{Fe}} \rangle_M) \quad (9b)$$

$$\delta E^F = \frac{1}{2} \Delta \alpha : [\mathbf{F}_{\text{Fe}} - \langle \mathbf{F}_{\text{Fe}} \rangle_M] \quad (9c)$$

where $[\mathbf{F}_{\text{Fe}}]_{kl} = F_{\text{Fe}}^{k,l} = E_{\text{Fe}}^k E_{\text{Fe}}^l$, $k, l = 1, 2, 3$, is the electric field tensor and the colon in (9c) denotes tensor contraction. Hence, the reorganization free energy λ_M^{var} can be written as a sum of potential, field and cross term contributions,

$$\lambda_M^{\text{var}} = \frac{\langle (\delta E)^2 \rangle_M}{2k_B T} = \lambda_M^{\text{var,V}} + \lambda_M^{\text{var,F}} + \lambda_M^{\text{var,VF}} \quad (10)$$

where

$$\lambda_M^{\text{var,V}} = \frac{\langle (\delta E^V)^2 \rangle_M}{2k_B T} \quad (11a)$$

$$\lambda_M^{\text{var,F}} = \frac{\langle (\delta E^F)^2 \rangle_M}{2k_B T} \quad (11b)$$

$$\lambda_M^{\text{var,VF}} = \frac{\langle \delta E^V \delta E^F \rangle_M}{k_B T} \quad (11c)$$

and the Stokes reorganization free energy as a sum of potential and field contribution,

$$\lambda^{\text{st}} = \frac{1}{2} (\langle \Delta E \rangle_{\text{R}} - \langle \Delta E \rangle_{\text{O}}) = \lambda^{\text{st,V}} + \lambda^{\text{st,F}} \quad (12)$$

where

$$\lambda^{\text{st},V} = \frac{1}{2}e(\langle V_{\text{Fe}} \rangle_{\text{R}} - \langle V_{\text{Fe}} \rangle_{\text{O}}) \quad (13a)$$

$$\lambda^{\text{st},F} = \frac{1}{4}\Delta\boldsymbol{\alpha} : [\langle \mathbf{F} \rangle_{\text{R}} - \langle \mathbf{F} \rangle_{\text{O}}] \quad (13b)$$

The reorganization free energies for the linear polarizability model are summarized in Tab. 2. They are very similar to the reorganization free energies obtained from the PMM method. Most importantly in the current context, the variance reorganization free energies (10), $\lambda_{\text{R}}^{\text{var}} = 1.33$ eV and $\lambda_{\text{O}}^{\text{var}} = 1.30$, are only slightly larger than the Stokes reorganization free energy (12), $\lambda^{\text{st}} = 1.03$ eV. A difference as large as reported in by MDM (up to a factor 1.7)³¹ is not observed. In Fig. 2 we further break down the total energy gap distribution in the contributions coming from the potential, electric field and cross term - as one can clearly see the contribution from the electrostatic potential fluctuations to reorganization free energy is dominating (88%, averaged over R and O) while the contributions from the field fluctuations (3%) and cross terms (8%) are relatively small.

In the following we analyze the discrepancy between our results and the ones of MDM. First we consider the distribution of the potential, V_{Fe} at the Fe site in Fig. 3a. As already noted by MDM, their potential distributions are rather similar to ours (Figure 3 in Ref. 31, reproduced here in Fig. 3a for our MD dataset “QM2/SF1”), which means that the potential distributions are not the cause for the discrepancy. Next we consider the polarizability tensors (7)-(8). The eigenvalues and eigenvectors of $\boldsymbol{\alpha}_M$ and $\Delta\boldsymbol{\alpha}$, as obtained from Gaussian (ZINDO/S) calculations, are summarized in Tab. 3. The eigenvectors of $\Delta\boldsymbol{\alpha}$ are shown as blue arrows in Fig. 1 and labeled in order of decreasing eigenvalues from “1” to “2” to “3”. We find that the polarizability in the heme-plane (approximately spanned by **1** and **2**) is significantly larger for the reduced than for the oxidized state, resulting in a polarizability difference between the two redox states of about 35-40 Å³. The polarizability and polarizability difference in the direction orthogonal to the heme plane (approximately

in direction **3**) is an order of magnitude smaller. These results are again similar to the ones reported by MDM,³¹ which means that the discrepancy can only come from the electric field at the Fe site, \mathbf{E}_{Fe} .

The distribution of the magnitude of the electric field, $|\mathbf{E}_{\text{Fe}}|$, and the components along the directions **1**, **2** and **3** are shown in Fig. 3b. The average electric field vector is indicated in magenta in Fig. 1. We find that the largest field component is in the direction where the polarizability difference $\Delta\alpha$ between reduced and oxidized states is the largest (direction **1**, approximately in the heme plane). This again is in agreement with MDM. However, the electric field distribution generated from MDM’s MD simulation is significantly broader, in particular for the reduced state, and reaches high values of up to 0.6 V/Å, compared to only 0.5 V/Å in our simulations (see Fig. 3b). Moreover, MDM observed a double-peak for the field distribution, possibly originating from protein conformational fluctuations that is not present in our MD simulations (see SI for structure-related data and further discussion). While this difference does not appear large at first sight, we note that the field-contribution to variance reorganization free energy, $\lambda_M^{\text{var},\text{F}}$ of (11b), is extremely sensitive to the magnitude of the field in the direction where the polarizability difference is large. This is because it is proportional to the square of gap fluctuations due to the field, δE^{F} , and the latter is proportional to the fluctuations of the squared field strength along the direction with high polarizability difference, see (9c). Indeed, we found that the estimated difference in the field fluctuations between MDM’s and our data, about 0.1 V/Å, has a major effect in variance reorganization free energy that is large enough to account for the discrepancy between MDM and our results.

Conclusions

In conclusion, using three different models for electronic polarizability of the heme cofactor, from the simplest linear polarizability/MM model, to QM(PMM)/MM to the most accurate,

full QM(DFT)/MM electrostatic embedding (investigated in our previous work), we do not observe in any of these computational models the large variance reorganization free energy reported by MDM. All methods give consistent results and the unfortunate claim made in Ref. 31 that our handling of the electric field was erroneous is untrue. We have traced back the discrepancy between MDM and our simulation to the significantly broader electric field distribution at the Fe site in their simulation featuring a double peak and reaching high electric fields of up to 0.6 V/Å. To put this number in perspective, the threshold field for dissociation of O-H bonds in liquid water was found to be 0.35 V/Å,⁴³ though the internal fields might be higher. Such large electric fields and field fluctuations are not supported by our ≈ 250 ns long MD simulations, neither with CHARMM nor with the AMBER force field.³² Therefore, our conclusion in Ref. 32 that there is no support for significant non-ergodic effects in cytochrome c on that time scale remains unchanged.

What becomes clear from many simulation studies in our group is that the effect of electronic polarization of the environment (here protein and water) needs to be included in the calculations.^{1,17,44–51} Otherwise reorganization free energy is strongly overestimated compared to experimentally determined values from photoemission spectroscopy and electrochemistry, not only for proteins but also for simple aqueous transition metal ion complexes $\text{Ru}(\text{bpy})_3^{2+/3+}$,⁴⁴ $\text{Mn}^{2+/3+}$ ⁴⁵ and $\text{Fe}^{2+/3+}$.⁴⁶ It would be hard to imagine that electronic polarizability of the environment is important for these simpler systems but not for proteins, or even more so, that non-ergodic effects instead of solvent electronic polarizability would lower the reorganization free energy in these systems to values in agreement with experiment, in particular when considering the very rigid nature of the $\text{Ru}(\text{bpy})_3^{2+/3+}$ -ion.

Acknowledgement

Z.F. was supported by the Czech Science Foundation (project 20-02067Y), X.J. was supported by a Ph.D. studentship cosponsored by the Chinese Scholarship Council and Univer-

sity College London. Via our membership of the UK's HEC Materials Chemistry Consortium, which is funded by EPSRC (EP/L000202, EP/R029431), this work used the ARCHER UK National Supercomputing Service (<http://www.archer.ac.uk>). We are grateful to the UK Materials and Molecular Modelling Hub for computational resources, which is partially funded by EPSRC (EP/P020194/1) as well as computational resources supplied by the project "e-Infrastruktura CZ" (e-INFRA LM2018140) provided within the program Projects of Large Research, Development and Innovations Infrastructures.

Supporting Information Available

Discussion of the reduced / oxidized protein structure, MD snapshots, RMSF and RMSD, XYZ coordinates of the active site in reduced and oxidized state, diagonal dipole moments obtained by ZINDO/S calculations on the active site. This material is available free of charge via the Internet at <http://pubs.acs.org/>.

Table 1: Energetics for oxidation of cytochrome c as obtained from QM(PMM)/MM calculations with diagonal transition moment matrix elements μ_{ii} (dipole moments) included or set to zero. All values in eV.

	This work ^a		MDM ^g
	μ_{ii} included	$\mu_{ii}=0$ ^f	μ_{ii} included
$\langle \Delta E \rangle_{\text{R}}^b$	3.28		
$\langle \Delta E \rangle_{\text{O}}^b$	1.23		
$\langle \delta E^2 \rangle_{\text{R}}^{1/2 \ c}$	0.25	0.25	
$\langle \delta E^2 \rangle_{\text{O}}^{1/2 \ c}$	0.25	0.25	
$\lambda_{\text{R}}^{\text{var} \ d}$	1.27	1.23	2.34
$\lambda_{\text{O}}^{\text{var} \ d}$	1.29	1.24	3.10
$\lambda^{\text{st} \ e}$	1.03	1.00	1.20

^a Calculated for QM2/SF1 MD sample of Ref. 32. ^b Thermal average of the vertical energy gap (3) sampled in reduced (R) or oxidized (O) state trajectories of aqueous cytochrome c. ^c Root-mean-square-fluctuations of vertical energy gap (3). ^d Variance reorganization free energy, $\lambda_M^{\text{var}} = \langle \delta E^2 \rangle_M / (2k_{\text{B}}T)$, $M = \text{R}, \text{O}$, $\delta E = \Delta E - \langle \Delta E \rangle_M$, ΔE from (3). ^e Stokes reorganization free energy, $\lambda^{\text{st}} = (\langle \Delta E \rangle_{\text{R}} - \langle \Delta E \rangle_{\text{O}}) / 2$, ΔE from (3). ^f Ref. 32. ^g Ref. 31

Table 2: Energetics for oxidation of cytochrome c as obtained from the linear polarizability model. All values in eV.

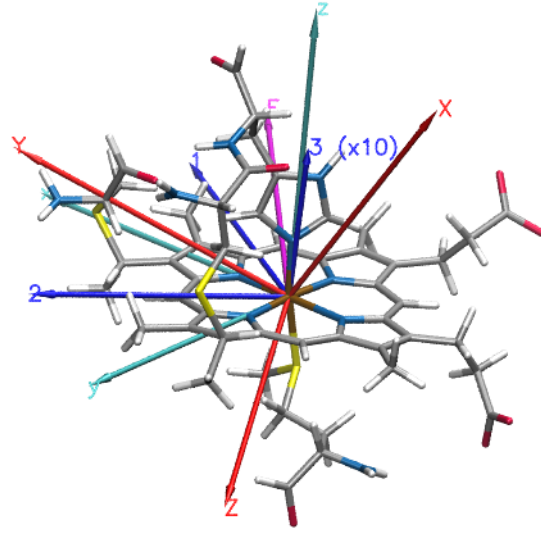
	This work ^a		MDM ⁿ	
	$M = R$	$M = O$	$M = R$	$M = O$
$\langle V_{Fe} \rangle_M^b$	3.29	1.33		
$\langle (\delta E)^2 \rangle_M^{1/2 \ c}$	0.26	0.25		
$\langle (\delta E^V)^2 \rangle_M^{1/2 \ d}$	0.24	0.24		
$\langle (\delta E^F)^2 \rangle_M^{1/2 \ e}$	0.05	0.04		
$\langle \delta E^V \delta E^F \rangle_M^{1/2 \ f}$	0.06	0.05		
$\lambda_M^{\text{var } g}$	1.33	1.30	2.15	1.84
$\lambda_M^{\text{var,V } h}$	1.14	1.18		
$\lambda_M^{\text{var,F } i}$	0.05	0.03		
$\lambda_M^{\text{var,VF } j}$	0.13	0.09		
$\lambda^{\text{st } k}$		1.03		1.17
$\lambda^{\text{st,V } l}$		0.98		
$\lambda^{\text{st,F } m}$		0.05		

^a Calculated for QM2/SF1 MD sample of Ref. 32. ^b Mean electrostatic potential at the Fe site. ^c Root-mean-square-fluctuations (RMSF) of total energy gap (9a). ^d RMSF of electrostatic potential contribution (9b). ^e RMSF of electric field contribution (9c). ^f Cross term of potential and field contribution. ^g Variance reorganization free energy (10). ^h Electrostatic potential energy contribution to ^f (11a). ⁱ Electric field contribution to ^f (11b). ^j Cross-term contribution to ^f (11c). ^k Stokes reorganization free energy (12). ^l Electrostatic potential energy contribution to ^j (13a). ^m Electric field contribution to ^j (13b). ⁿ Ref. 31.

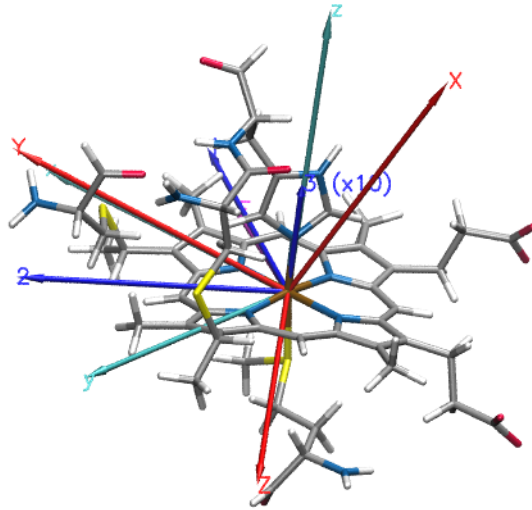
Table 3: Polarizability tensor, eigenvalues and eigenvectors in the reduced and oxidized geometry of the heme c cofactor. All values for polarizability are in units of \AA^3 .

	This work						MDM ^g	
	Geometry of R			Geometry of O			α_R^a	α_O^a
	α_R^a	α_O^a	$\Delta\alpha^b$	α_O^a	α_R^a	$\Delta\alpha^b$		
α_1^c	80.257	44.052	41.788	44.754	79.827	39.392	81.2	37.4
α_2^c	77.806	36.237	36.087	38.121	77.385	35.049	77.6	31.7
α_3^c	3.670	1.542	2.027	2.226	3.717	1.386	3.7	1.1
$e_1^{\alpha_1^c d}$	-0.358	-0.289	-0.464	-0.312	-0.328	-0.313		
$e_2^{\alpha_1^c d}$	0.919	0.879	0.305	0.913	0.931	0.213		
$e_3^{\alpha_1^c d}$	0.166	0.379	-0.832	0.262	0.161	-0.925		
$e_1^{\alpha_2^c d}$	0.351	0.398	-0.207	0.235	0.236	-0.273		
$e_2^{\alpha_2^c d}$	-0.032	-0.250	0.876	-0.193	-0.084	0.913		
$e_3^{\alpha_2^c d}$	0.936	0.883	0.436	0.953	0.968	0.303		
$e_1^{\alpha_3^c d}$	0.865	0.871	0.861	0.920	0.915	0.910		
$e_2^{\alpha_3^c d}$	0.394	0.406	0.374	0.359	0.355	0.347		
$e_3^{\alpha_3^c d}$	-0.311	-0.277	-0.343	-0.154	-0.192	-0.228		
α^e	53.911	27.277	26.634	28.367	53.643	25.276	54.2	23.4
γ^f	75.391	39.191	37.240	39.630	74.919	36.032	75.8	33.9

^a Eq. 8. ^b Eq. 7. ^c Eigenvalues of polarizability tensor. ^d Normalized eigenvectors corresponding to α_i in the (\mathbf{X} , \mathbf{Y} , \mathbf{Z}) coordinate frame. ^e Average polarizability, $\alpha = \text{Tr}[\boldsymbol{\alpha}]/3$ ^f Anisotropy of polarizability, $\gamma^2 = (3\text{Tr}[\boldsymbol{\alpha}^2] - \text{Tr}[\boldsymbol{\alpha}]^2)/2$. ^g Ref. 31.



(a)



(b)

Figure 1: Structure and coordinate frames for the heme c cofactor model (a) in the reduced and (b) in the oxidized state. Gaussian Cartesian axes ($\mathbf{X}, \mathbf{Y}, \mathbf{Z}$) used in ZINDO/S calculations of electronic transition dipole moment matrix elements and polarizability are shown in red, local heme coordinate axes ($\mathbf{x}, \mathbf{y}, \mathbf{z}$) used for structure alignment are shown in cyan and eigenvectors of polarizability difference $\Delta\alpha$ ($\mathbf{1}, \mathbf{2}, \mathbf{3}$) are shown in blue. The length of the eigenvectors is proportional to the corresponding eigenvalues (eigenvector 3 is scaled by factor of 10). The average electric field vectors are indicated in magenta in (a) and (b). They take values $\langle \mathbf{E}_{\text{Fe}} \rangle_{\text{R}} = (0.348, -0.077, 0.074)$ V/Å and $\langle \mathbf{E}_{\text{Fe}} \rangle_{\text{O}} = (0.229, -0.029, -0.047)$ V/Å in the (1, 2, 3) coordinate frame.

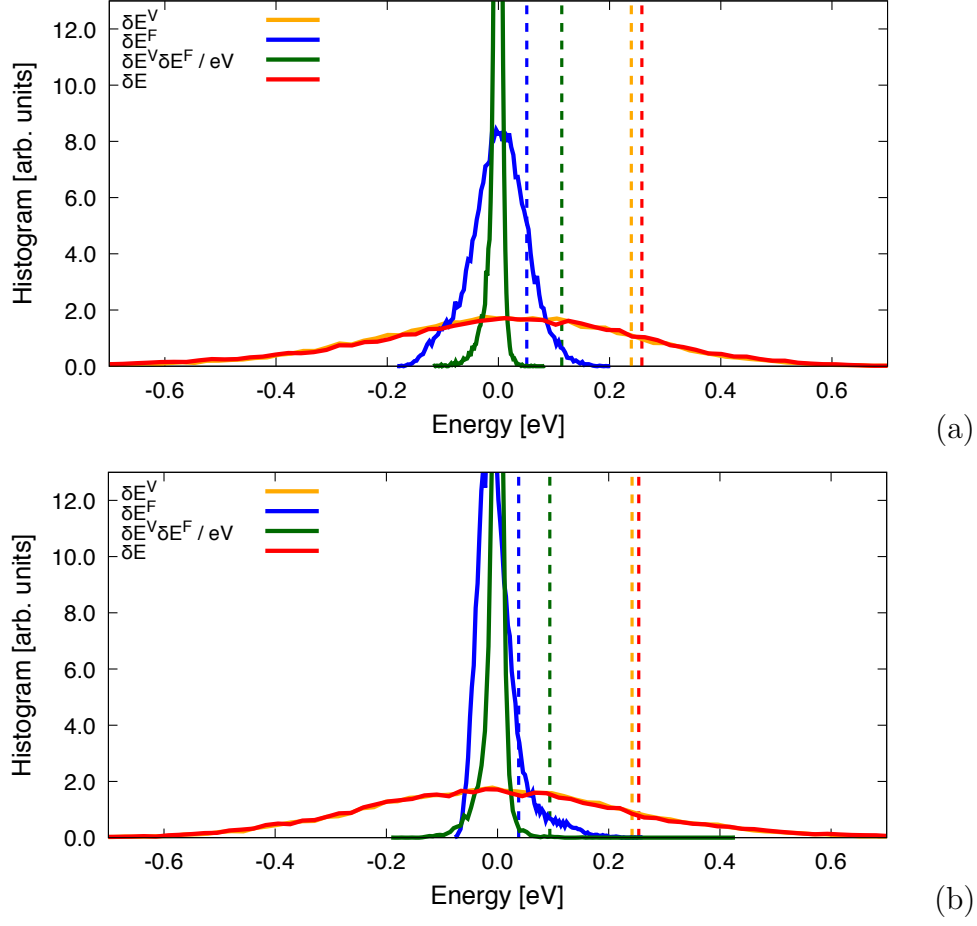


Figure 2: Energy gap distributions for oxidation of solvated cytochrome c. The distributions are for the QM2/SF1 sample of Ref. 32 obtained from MD simulation in reduced state (a) and oxidized state (b) of the protein. Distribution of total energy gap fluctuations δE (Eq. 9a, red) and its contributions δE^V (Eq. 9b, orange), δE^F (Eq. 9c, blue) and $\delta E^V \delta E^F / \text{eV}$ (green). The root-mean-square fluctuations of the energy gaps, $\langle (\delta E)^2 \rangle^{1/2}$, $\langle (\delta E^V)^2 \rangle^{1/2}$, $\langle (\delta E^F)^2 \rangle^{1/2}$ and $\langle 2\delta E^V \delta E^F \rangle^{1/2}$ are shown by vertical dashed lines in the corresponding colors.

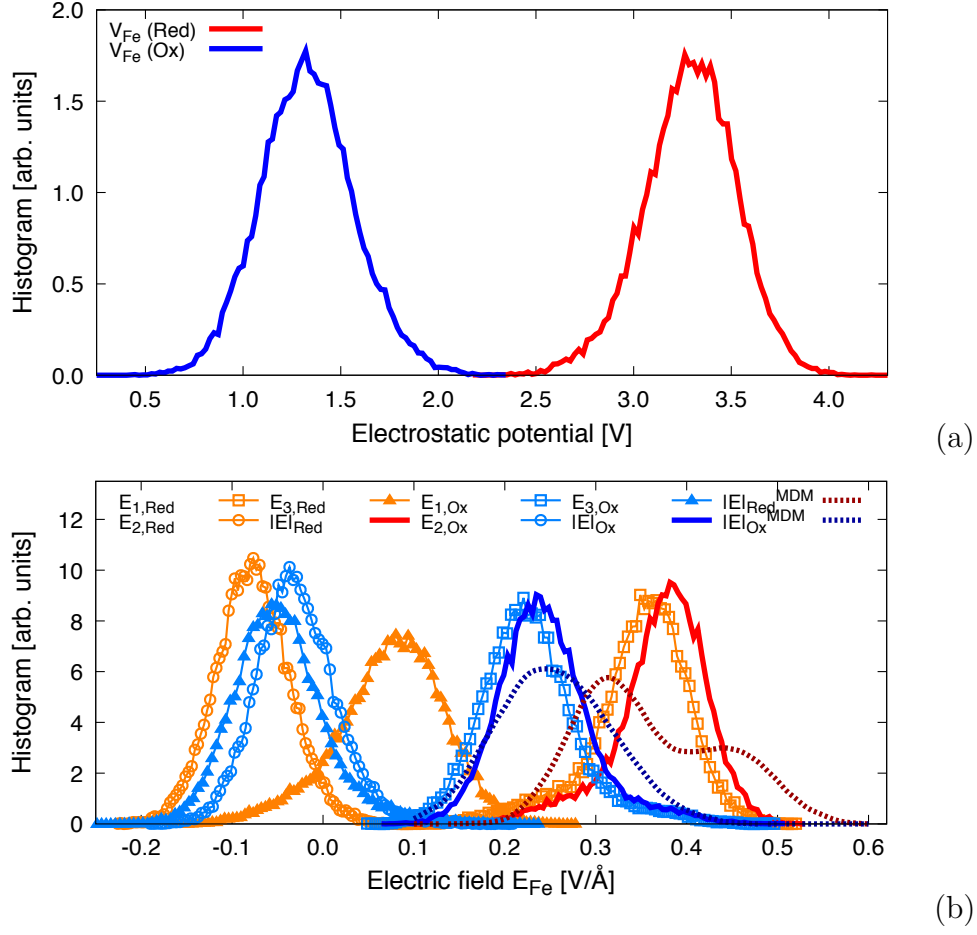


Figure 3: Distribution of (a) electrostatic potential V_{Fe} and (b) electric field \mathbf{E}_{Fe} in solvated cytochrome c. The distributions are for the QM2/SF1 sample of Ref. 32 obtained from MD simulation in reduced state (red lines) and oxidized state of the protein (blue lines). In (b), the magnitude of the electric field vector, $|\mathbf{E}_{\text{Fe}}|$ (solid lines), and the components in the directions of the eigenvectors of the polarizability difference tensor ($\mathbf{1}$, $\mathbf{2}$, $\mathbf{3}$) are shown (symbols). The field distributions of MDM (Ref. 31) are shown for comparison (dashed lines).

References

- (1) Blumberger, J. Recent advances in the theory and molecular simulation of biological electron transfer reactions. *Chem. Rev.* **2015**, *115*, 11191–11238.
- (2) Moser, C. C.; Keske, J. M.; Warncke, K.; Farid, R. S.; Dutton, P. L. Nature of biological electron transfer. *Nature* **1992**, *355*, 796–802.
- (3) Page, C. C.; Moser, C. C.; Chen, X.; Dutton, P. L. Natural engineering principles of electron tunnelling in biological oxidation-reduction. *Nature* **1999**, *402*, 47–52.
- (4) Gray, H. B.; Winkler, J. R. Electron tunneling through proteins. *Quart. Rev. Biophys.* **2003**, *36*, 341–372.
- (5) Beratan, D. N.; Skourtis, S. S.; Balabin, I. A.; Balaeff, A.; Keinan, S.; Venkatramani, R.; Xiao, D. Steering Electrons on Moving Pathways. *Acc. Chem. Res.* **2009**, *42*, 1669–1678.
- (6) Skourtis, S. S.; Waldeck, D. H.; Beratan, D. N. Fluctuations in Biological and Bioinspired Electron-Transfer Reactions. *Annu. Rev. Phys. Chem.* **2010**, *61*, 461–485.
- (7) Venkatramani, R.; Keinan, S.; Balaeff, A.; Beratan, D. N. Nucleic Acid Charge Transfer: Black, White and Gray. *Coord. Chem. Rev.* **2011**, *255*, 635–648.
- (8) Saen-Oon, S.; M, F. L.; Guallar, V. Electron transfer in proteins: theory, applications and future perspectives. *Phys. Chem. Chem. Phys.* **2013**, *15*, 15271–15285.
- (9) Kubař, T.; Elstner, M. A hybrid approach to simulation of electron transfer in complex molecular systems. *J. R. Soc. Interface* **2013**, *10*, 20130415.
- (10) Matyushov, D. V. Protein electron transfer: Dynamics and statistics. *J. Chem. Phys.* **2013**, *139*, 025102–12.
- (11) Skourtis, S. S. In *Quantum Effects in Biology*; Masoud Mohseni, G. S. E., Yasser Omar, Plenio, M. B., Eds.; Cambridge University Press, 2014; Chapter 9, pp 198–217.

- (12) Winkler, J. R.; Gray, H. B. Electron Flow through Metalloproteins. *Chem. Rev.* **2014**, *114*, 3369–3380.
- (13) Beratan, D. N.; Liu, C.; Migliore, A.; Polizzi, N. F.; Skourtis, S. S.; Zhang, P.; Zhang, Y. Charge Transfer in Dynamical Biosystems, or The Treachery of (Static) Images. *Acc. Chem. Res.* **2015**, *48*, 474–481.
- (14) Narth, C.; Gillet, N.; Cailliez, F.; Levy, B.; de la Lande, A. Electron Transfer, Decoherence, and Protein Dynamics: Insights from Atomistic Simulations. *Acc. Chem. Res.* **2015**, *48*, 1090–1097.
- (15) de la Lande, A.; Gillet, N.; Chen, S.; Salahub, D. R. Progress and challenges in simulating and understanding electron transfer in proteins. *Arch. Biochem. Biophys.* **2015**, *582*, 28–41.
- (16) Blumberger, J. Free energies for biological electron transfer from QM/MM calculation: method, application and critical assessment. *Phys. Chem. Chem. Phys.* **2008**, *10*, 5651–5667.
- (17) Jiang, X.; Futera, Z.; Ali, M. E.; Gajdos, F.; Rudorff, G. F. v.; Carof, A.; Breuer, M.; Blumberger, J. Cysteine linkages accelerate electron flow through tetra-heme protein STC. *J. Am. Chem. Soc.* **2017**, *139*, 17237–17240.
- (18) Jiang, Y.; Geng, H.; Li, W.; Shuai, Z. Understanding Carrier Transport in Organic Semiconductors: Computation of Charge Mobility Considering Quantum Nuclear Tunneling and Delocalization Effects. *J. Chem. Theor. Comput.* **2019**, DOI: [10.1021/acs.jctc.8b00779](https://doi.org/10.1021/acs.jctc.8b00779).
- (19) Carter, E. A.; Hynes, J. T. Solute-dependent solvent force constants for ion pairs and neutral pairs in a polar solvent. *J. Phys. Chem.* **1989**, *93*, 2184–2187.

- (20) Blumberger, J. $\text{Cu}_{\text{aq}}^+/\text{Cu}_{\text{aq}}^{2+}$ Redox Reaction Exhibits Strong Nonlinear Solvent Response Due to Change in Coordination Number. *J. Am. Chem. Soc.* **2008**, *130*, 16065–16068.
- (21) Vuilleumier, R.; Tay, K. A.; Jeanmairet, G.; Borgis, D.; Boutin, A. Extension of Marcus picture for electron transfer reactions with large solvation changes. *J. Am. Chem. Soc.* **2012**, *134*, 2067–2074.
- (22) Blumberger, J.; Tavernelli, I.; Klein, M. L.; Sprik, M. Diabatic free energy curves and coordination fluctuations for the aqueous $\text{Ag}^+/\text{Ag}^{2+}$ redox couple: A biased Born-Oppenheimer molecular dynamics investigation. *J. Chem. Phys.* **2006**, *124*, 064507–12.
- (23) Small, D. W.; Matyushov, D. V.; Voth, G. A. The theory of electron transfer reactions: What may be missing? *J. Am. Chem. Soc.* **2003**, *125*, 7470–7478.
- (24) LeBard, D. N.; Matyushov, D. V. Protein-water electrostatics and principles of bioenergetics. *Phys. Chem. Chem. Phys.* **2010**, *12*, 15335–15348.
- (25) LeBard, D. N.; Kapko, V.; Matyushov, D. V. Energetics and kinetics of primary charge separation in bacterial photosynthesis. *J. Phys. Chem. B* **2008**, *112*, 10322–10342.
- (26) LeBard, D. N.; Matyushov, D. V. Energetics of bacterial photosynthesis. *J. Phys. Chem. B* **2009**, *113*, 12424–12437.
- (27) Matyushov, D. Protein electron transfer: is biology (thermo)dynamic? *J. Phys.: Condens. Matter* **2015**, *27*, 473001.
- (28) Dinpajoo, M.; Martin, D. R.; Matyushov, D. V. Polarizability of the active site of cytochrome c reduces the activation barrier for electron transfer. *Sci. Rep.* **2016**, *6*, 28152.
- (29) Seyedi, S. S.; Waskasi, M. M.; Matyushov, D. V. Theory and Electrochemistry of Cytochrome c. *J. Phys. Chem. B* **2017**, *121*, 4958–4967.

- (30) Seyedi, S.; Matyushov, D. V. Termination of Biological Function at Low Temperatures: Glass or Structural Transition? *J. Phys. Chem. Lett.* **2018**, *9*, 2359–2366.
- (31) Martin, D. R.; Dinpajoo, M.; Matyushov, D. V. Polarizability of the Active Site in Enzymatic Catalysis: Cytochrome c. *J. Phys. Chem. B* **2019**, *123*, 10691.
- (32) Jiang, X.; Futera, Z.; Blumberger, J. Ergodicity-Breaking in Thermal Biological Electron Transfer? Cytochrome C Revisited. *J. Phys. Chem. B* **2019**, *123*, 7588–7598.
- (33) Banci, L.; Bertini, I.; Huber, J. G.; Spyroulias, G. A.; Turano, P. Solution structure of reduced horse heart cytochrome c. *J. Biol. Inorg. Chem.* **1999**, *4*, 21–31.
- (34) Feller, S. E.; Mackerell, A. D. An Improved Empirical Potential Energy Function for Molecular Simulations of Phospholipids. *J. Phys. Chem. B* **2000**, *104*, 7510–7515.
- (35) Jorgensen, W. L.; Chandrasekhar, J.; Madura, J. D.; Impey, R. W.; Klein, M. L. Comparison of simple potential functions for simulating liquid water. *J. Chem. Phys.* **1983**, *79*, 926–935.
- (36) Phillips, J. C.; Braun, R.; Wang, W.; Gumbart, J.; Tajkhorshid, E.; Villa, E.; Chipot, C.; Skeel, R. D.; Kale, L.; Schulten, K. Scalable molecular dynamics with NAMD. *J. Comput. Chem.* **2005**, *26*, 1781.
- (37) Amadei, A.; Daidone, I.; Bortolotti, C. A. A general statistical mechanical approach for modeling redox thermodynamics: the reaction and reorganization free energies. *RSC Adv.* **2013**, *3*, 19657–19665.
- (38) Daidone, I.; Amadei, A.; Zaccanti, F.; Borsari, M.; Bortolotti, C. A. How the Reorganization Free Energy Affects the Reduction Potential of Structurally Homologous Cytochromes. *J. Phys. Chem. Lett.* **2014**, *5*, 1534–1540.
- (39) Aschi, M.; Spezia, R.; Nola, A. D.; Amadei, A. A first-principles method to model

- perturbed electronic wavefunctions: the effect of an external homogeneous electric field. *Chem. Phys. Lett.* **2001**, *344*, 374–380.
- (40) Bortolotti, C. A.; Amadei, A.; Aschi, M.; Borsari, M.; Corni, S.; Sola, M.; Daidone, I. The Reversible Opening of Water Channels in Cytochrome c Modulates the Heme Iron Reduction Potential. *J. Am. Chem. Soc.* **2012**, *134*, 13670–13678.
- (41) Zanetti-Polzi, L.; Galdo, S. D.; Daidone, I.; D’Abramo, M.; Barone, V.; Aschi, M.; Amadei, A. Extending the perturbed matrix method beyond the dipolar approximation: comparison of different levels of theory. *Phys. Chem. Chem. Phys.* **2018**, *20*, 24369–24378.
- (42) Frisch, M. J.; Trucks, G. W.; Schlegel, H. B.; Scuseria, G. E.; Robb, M. A.; Cheeseman, J. R.; Scalmani, G.; Barone, V.; Petersson, G. A.; Nakatsuji, H. et al. Gaussian16 Revision C.01. 2016; Gaussian Inc. Wallingford CT.
- (43) Saitta, A. M.; Saija, F.; Giaquinta, P. V. Ab Initio Molecular Dynamics Study of Dissociation of Water Under an Electric Field. *Phys. Rev. Lett.* **2012**, *108*, 207801.
- (44) Seidel, R.; Faubel, M.; Winter, B.; Blumberger, J. Single-ion reorganization free energy of aqueous $\text{Ru}(\text{bpy})_3^{2+/3+}$ and $\text{Ru}(\text{H}_2\text{O})_6^{2+/3+}$ from photoemission spectroscopy and density functional molecular dynamics simulation. *J. Am. Chem. Soc.* **2009**, *131*, 16127–16137.
- (45) Moens, J.; Seidel, R.; Geerlings, P.; Faubel, M.; Winter, B.; Blumberger, J. Energy Levels and Redox Properties of Aqueous $\text{Mn}^{2+/3+}$ from Photoemission Spectroscopy and Density Functional Molecular Dynamics Simulation. *J. Phys. Chem. B* **2010**, *114*, 9173–9182.
- (46) Seidel, R.; Thurmer, S.; Moens, J.; Geerlings, P.; Blumberger, J.; Winter, B. Valence photoemission spectra of aqueous $\text{Fe}^{2+/3+}$ and $[\text{Fe}(\text{CN})_6]^{4-/3-}$ and their interpretation by DFT calculations. *J. Phys. Chem. B* **2011**, *115*, 11671.

- (47) Oberhofer, H.; Blumberger, J. Insight into the mechanism of the Ru^{2+} - Ru^{3+} electron self-exchange reaction from quantitative rate calculations. *Angew. Chem. Int. Ed.* **2010**, *49*, 3631–3634.
- (48) Tipmanee, V.; Oberhofer, H.; Park, M.; Kim, K. S.; Blumberger, J. Prediction of Reorganization Free Energies for Biological Electron Transfer: A Comparative Study of Ru-Modified Cytochromes and a 4-Helix Bundle Protein. *J. Am. Chem. Soc.* **2010**, *132*, 17032–17040.
- (49) Blumberger, J.; McKenna, K. Constrained Density Functional Theory Applied to Electron Tunnelling between Defects in MgO. *Phys. Chem. Chem. Phys.* **2013**, *15*, 2184–2196.
- (50) Wonderen, J. H. v.; Hall, C. R.; Jiang, X.; Adamczyk, K.; Carof, A.; Heisler, I.; Piper, S. E. H.; Clarke, T. A.; Watmough, N. J.; Sazanovich, I. V. et al. Ultra-fast light-driven electron transfer in a Ru(II)tris(bipyridine)-labelled multiheme cytochrome. *J. Am. Chem. Soc.* **2019**, *141*, 15190–15200.
- (51) Jiang, X.; Burger, B.; Gajdos, F.; Bortolotti, C.; Futera, Z.; Breuer, M.; Blumberger, J. Kinetics of trifurcated electron flow in the decaheme bacterial proteins MtrC and MtrF. *Proc. Nat. Acad. Sci. USA* **2019**, *116*, 3425–3430.

Graphical TOC Entry

